Rapid Communications

Triplet superconductivity in the Dirac semimetal germanene on a substrate

Domenico Di Sante,[*,†] Xianxin Wu,[*,‡] Mario Fink, Werner Hanke, and Ronny Thomale
Institut für Theoretische Physik und Astrophysik, Universität Würzburg, Am Hubland Campus Süd, Würzburg 97074, Germany

(Received 16 October 2018; published 13 May 2019)

The success of graphene and its emerging Dirac physics has stimulated the quest for versatile and tunable electronic properties in atomically thin systems, leading to the discovery of various chemical classes of two-dimensional (2D) compounds. In particular, honeycomb lattices of group-IV elements, such as silicene and germanene, have been found experimentally. Whether it is a necessity of synthesis or a desired feature for application purposes, most 2D materials demand a supporting substrate. In this Rapid Communication, by combining *ab initio* simulations with multiorbital functional renormalization group analysis of Fermi surface instabilities, we highlight the constructive impact of substrates to enable the realization of exotic electronic quantum states of matter, where the buckling emerges as the decisive material parameter adjustable by the commensuration. At the example of germanene deposited on MoS_2, an experimentally characterized superstructure, we find that the coupling between the monolayer and the substrate, together with the buckled hexagonal geometry, conspire to provide a highly suited scenario for unconventional triplet superconductivity.

DOI: 10.1103/PhysRevB.99.201106

I. INTRODUCTION

Material synthesis in two spatial dimensions is one of the rising fields of contemporary condensed matter physics. Initiated by the exfoliation and substrate-assisted growth of graphene [1,2], complementary techniques such as refined sputtering and molecular beam epitaxy are significantly broadening the scope of two-dimensional (2D) material classes, which by themselves are considered promising hosts for exotic electronic quantum states of matter. This includes not only topological quantum matter such as quantum spin Hall (QSH) insulators and Chern insulators [3,4], but also unconventional superconductors, which has climaxed in the discovery of superconductivity in doped twisted bilayer graphene [5,6].

For 2D superconductors, an overarching principle is to attempt to access a high density of states (DOS) at the Fermi level, which constitutes a promising setup for high critical temperatures. For graphene, at a filling factor corresponding to ∼13% of doping concentration, a van Hove singularity (vHs) in the DOS was proposed to drive a substantial enhancement of interaction effects [7]. One striking consequence is the predicted appearance of $d + id$-wave superconductivity [8–10], which would allow one to enter the rich phenomenology of topological superconductors. Several attempts have been made to dope graphene to the vH point by chemical doping [11]. Notwithstanding the efforts, so far no evidence of the observation of unconventional superconductivity has been reported. This is presumably because of the added disorder capping the large DOS at the vHs, which, in graphene, only shows up (see Fig. 1) at energies away from the Fermi level at half filling comparable to the nearest-neighbor hopping parameter (∼3 eV). As a consequence, one guiding principle for improvement is to identify alternative scenarios in which vH filling can be achieved at lower doping.

Silicene and germanene as 2D-Xenes exhibit larger bond lengths than graphene and prevent the atoms from forming strong π bonds, yielding a smaller nearest-neighbor hopping (∼1 eV). The growth of such systems requires proper substrates and templates. Aiming at QSH insulator phases, 2D-Xenes may be suited because of their heavy constituent atoms and a larger spin-orbit-mediated topological band gap [12–14]. Xene geometric reconstruction has been reported for metallic substrates Ag, Au, Pt, Al, and Ir [15–18], as well as less interacting substrates such as MoS_2 and AlN [15,19,20]. Common reconstructed phases are $\sqrt{3} \times \sqrt{3}$, $\sqrt{7} \times \sqrt{7}$, 2×2, but also the larger 3×3 and 5×5 setting [15]. Bonding with the substrate and complex surface reconstructions render the analysis of realistic systems a challenging task from experiment and theory [21]. Furthermore, the strong monolayer/substrate interaction often avoids the QSH scenario in favor of, on first view, an undesirable metallic phase [20,22]. In light of unconventional superconductivity, however, the key insight of this Rapid Communication is that the presence of a substrate can drastically modify the low-energy physics of 2D-Xenes in an advantageous manner, as to create a different fermiology characterized by enlarged DOS already at pristine filling, and a vHs accessible upon moderate doping. As the graphene-type fermiology is fundamentally altered through the substrate, we find that substrate-supported 2D electronic structures establish an intriguing platform for unconventional Fermi surface instabilities in general, and superconductivity in particular. By germanene on MoS_2, we identify an electronic structure which promises to be preeminently suited for the observation of f-wave superconductivity, a state which has so far remained elusive in nature.

[*]These authors contributed equally to the work.
[†]domenico.disante@physik.uni-wuerzburg.de
[‡]xianxin.wu@physik.uni-wuerzburg.de

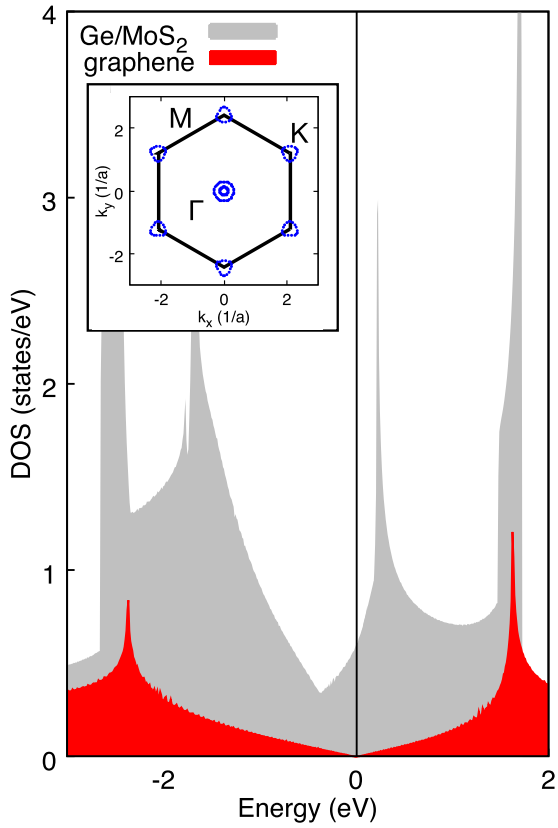

FIG. 1. Fermi surface and density of the states. Comparison between the DOS of graphene (red) and germanene/MoS_2 (gray). The Fermi level, corresponding to the vertical dashed line, is set to half filling in both cases, and separates the hole doping (left) from the electron doping (right) regimes. The inset shows the Fermi surface of germanene/MoS_2 in the absence of doping.

II. ELECTRONIC PROPERTIES

The peculiar properties of Ge/MoS_2 already become visible from a comparison of DOS against graphene (Fig. 1). Already at half filling, Ge/MoS_2 exhibits a sizable carrier density. Even more remarkably, however, the vHs, in particular the one on the electron-doped side, is shifted closer to half filling as compared to graphene. This observation is of general importance independent of the type of Fermi surface instability we are interested in, since all instability scales, from the viewpoint of weak coupling, are enhanced by an enlarged DOS at the Fermi level. As a next step, we analyze the detailed fermiology and general microscopic setting of Ge/MoS_2 in the vicinity of vH filling.

Figure 2(a) shows the established structural model for 5×5 germanene on 6×6 MoS_2 [20], while in Table I and in Ref. [23] we also report the cases of 3×3 germanene on 4×4 AlN/Ag(111) [19] and $\sqrt{3} \times \sqrt{3}R(30^\circ)$ germanene on $\sqrt{7} \times \sqrt{7}R(19.1^\circ)$ Au(111) [18]. We computed the supercell's band structure and unfolded it into the primitive Brillouin zone, obtaining the unfolding weights [red symbols in Fig. 2(b); see Ref. [23] for details]. When grown on MoS_2, the electronic states of germanene are weakly disturbed by the interaction with the substrate. The significant compressive lateral strain on the honeycomb lattice (∼5%), however, increases the buckling distortion up to 0.86 Å, and induces a crossing of the Fermi level around the Γ point by holelike bands (see also Ref. [23]), turning the system into a compensated Dirac semimetal phase with a finite DOS at the Fermi level. We develop a realistic tight-binding model able to reproduce the single-particle band structure of Ge/MoS_2 [24]. In Table I, we report our parameter fit to the *ab initio* results within a simplified nearest-neighbor (NN) approximation [gray bands in Fig. 2(c) for Ge/MoS_2]. Next-nearest-neighbor hoppings are delegated to the Supplemental Material [23]; as another step of refinement, instead of resorting to

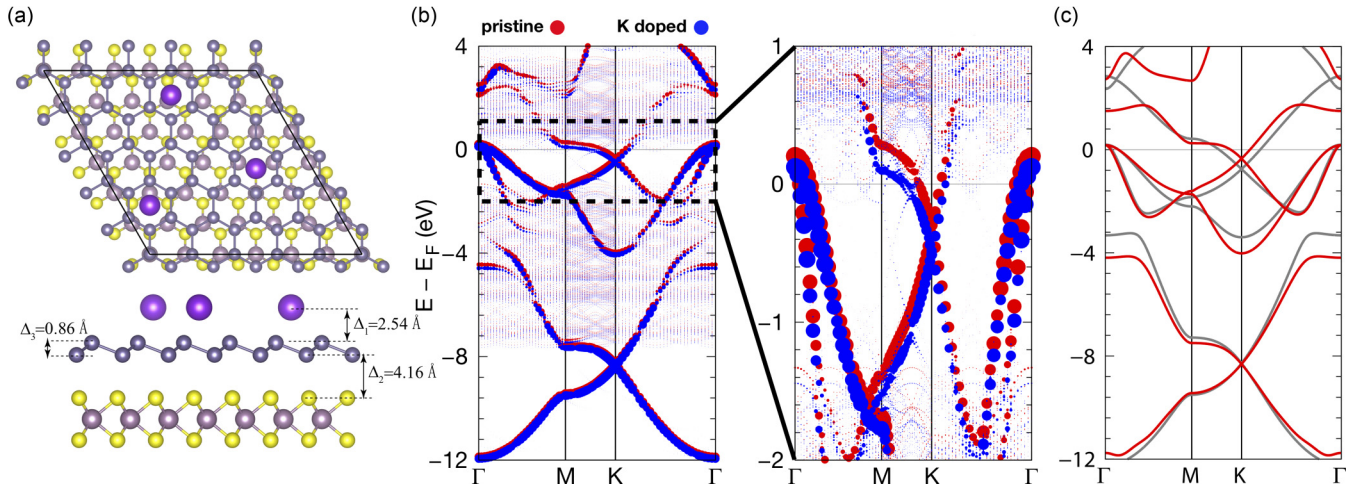

FIG. 2. First-principles calculations of realistic germanene/MoS_2. (a) Structural model for 5×5 germanene on 6×6 MoS_2, with the inclusion of potassium atoms to simulate chemical doping. (b) Density functional theory (DFT) band structure (wide energy range view on the left and zoom around the Fermi level on the right) of the superstructure in (a) along the high-symmetry lines of the 1×1 Brillouin zone. The red and blue circles highlight the weights of the unfolded electronic states for the pristine and K-doped system, respectively. (c) Band structure of the *ab initio* Wannier model (red) and the nearest-neighbor tight-binding (TB) Slater-Koster model with parameters listed in Table I and the Hamiltonian given in Ref. [23] (gray).

TABLE I. Structural and hopping parameters in the eight-band NN Slater-Koster tight-binding model. Δ_3 (Å) is the buckling parameter of the honeycomb lattice [see Fig. 2(a)], described also by the buckling angle θ (deg) between the Ge-Ge bond and the z direction normal to the surface. ϵ_s, $\epsilon_{p_{x,y}}$, and ϵ_{p_z} (eV) are the on-site energies of the s, p_x, p_y, and p_z orbitals, while $V_{ss\sigma}$, $V_{sp\sigma}$, $V_{pp\sigma}$, and $V_{pp\pi}$ (eV) parametrize the Slater-Koster transfer intergrals. DS, CDS, and M in the last column are acronyms for Dirac semimetal, compensated Dirac semimetal, and metallic phases of the ground state, respectively. The band structures for Ge/AlN/Ag(111) and Ge/Au(111) are shown in the Supplemental Material [23].

	Reconstruction	Δ_3	θ	ϵ_s	$\epsilon_{p_{x,y}}$	ϵ_{p_z}	$V_{ss\sigma}$	$V_{sp\sigma}$	$V_{pp\sigma}$	$V_{pp\pi}$	Phase
Ge/AlN/Ag(111)	$3\times 3/4\times 4$	0.70	107.3	−5.44	2.76	0.86	−1.8	2.5	3.3	−1.0	DS
Ge/MoS_2	$5\times 5/6\times 6$	0.86	111.4	−5.74	2.46	0.56	−2.0	2.5	3.3	−1.2	CDS
Ge/Au(111)	$\sqrt{3}\times\sqrt{3}/\sqrt{7}\times\sqrt{7}$	0.47	100.5	−6.24	1.96	0.06	−1.5	2.5	3.3	−1.2	M

a tight-binding fit, we also employ a full Wannier-function-based model [red bands in Fig. 2(c)], which we have used for our Fermi surface instability calculations.

In graphene, 0.5 electron doping per unit cell is needed to reach the vHs point. At the present stage of experimental capabilities, such a high electron doping is unavoidably accompanied by detrimental disorder effects. In Ge/MoS_2, as the vHs point is energetically closer to the Fermi level, the vHs can be reached upon doping of ∼0.2 electrons per unit cell, i.e., only 40% of the doping value needed for graphene. In Fig. 2(b), we show the band structure of Ge/MoS_2 upon doping by three alkali atoms per unit cell. This doping shifts the vHs close to the Fermi level (without much affecting the states around the Γ point) by providing 0.12 electrons, such that the vHs now is only 0.1 eV above the Fermi level.

The Fermi surface of Ge/MoS_2 doped to the vHs is shown in Fig. 3(a). It is almost circular and rather flat along the M-K line, which is in sharp contrast to the expected hexagonal shape for vH-doped graphene. In graphene, the nesting between opposite edges of the hexagonal Fermi surface promotes strong antiferromagnetic fluctuations around the M point, which in turn drive the $d+id$ pairing states [8–10]. In Ge/MoS_2, this nesting is absent due to the circular Fermi surface, and the dominant nesting (denoted by the arrow) promotes ferromagnetic fluctuations. This is evident from the intense $\mathbf{q}=\mathbf{0}$ peak in the momentum space distribution of the bare susceptibility shown in Fig. 3(b). Furthermore, the Fermi velocities of graphene and Ge/MoS_2 are different. For the former, the minimum of the Fermi velocity is localized around the M point, leading to a peaked DOS in its vicinity. For the latter, a high DOS is extended over a large fraction of the Fermi surface [see Fig. 3(a)], and any minimal reduction to the M points is no longer valid [8].

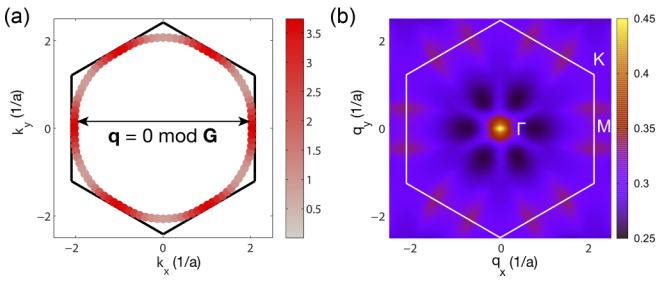

FIG. 3. Fermiology of germanene/MoS_2 at the vHs point. (a) Fermi surface and momentum distribution of the DOS [$\rho_{\mathbf{k}}\sim 1/|v_F(\mathbf{k})|$, with $v_F(\mathbf{k})$ the Fermi velocity] at the vHs energy. The arrow highlights the $\mathbf{q}=\mathbf{0}$ nesting vector up to a reciprocal lattice vector. (b) Momentum distribution of the RPA bare susceptibility (see Ref. [23]). The color bars are in eV Å and eV^{-1} units, respectively.

III. fRG CALCULATIONS

We adopt the functional renormalization group (fRG) approach to study Fermi surface instabilities, by starting from the bare many-body interaction

$$\begin{aligned} H_{\mathrm{int}} &= U\sum_{i\alpha} n_{i\alpha\uparrow}n_{i\alpha\downarrow} + U'\sum_{i,\alpha<\beta} n_{i\alpha}n_{i\beta} \\ &+ J\sum_{i,\alpha<\beta,\sigma\sigma'} c^\dagger_{i\alpha\sigma}c^\dagger_{i\beta\sigma'}c_{i\alpha\sigma'}c_{i\beta\sigma} \\ &+ J'\sum_{i,\alpha\neq\beta} c^\dagger_{i\alpha\uparrow}c^\dagger_{i\alpha\downarrow}c_{i\beta\downarrow}c_{i\beta\uparrow}, \end{aligned} \tag{1}$$

where $n_{i\alpha}=n_{\alpha\uparrow}+n_{\alpha\downarrow}$ with α and i the sublattice and orbital indices. Fourier transforming and integrating out the high-energy degrees of freedom determines the renormalized interaction described by the four-point function (4PF) $V_\Lambda(\mathbf{k}_1,\mathbf{k}_2,\mathbf{k}_3,\mathbf{k}_4)$ [25,26]. V_Λ diverges in some channels as the cutoff Λ approaches the Fermi surface, marking the onset of a leading instability [23]. The parametrization of germanene on MoS_2 (bandwidth $W\sim 20$ eV) serves as the starting, i.e., nonrenormalized, limit for our fRG study.

The interaction Hamiltonian we consider contains intra- and interorbital repulsion U and U', as well as Hund's rule coupling J and pair hopping J' [23]. For simplicity, in the absence of *ab initio* estimates of the interaction parameters, we choose the ansatz $U=U'+2J$, $U=2U'$, and $J=J'$, tuning the global scale such that the resulting maximum strength of the initial vertex function $V_{\Lambda=W}(\mathbf{k}_1,\mathbf{k}_2,\mathbf{k}_3,\mathbf{k}_4)$ for momenta on the Fermi surface is still located in the weak to intermediate coupling regime.

For a given instability characterized by some particle-particle- or particle-hole-like ordering field $O_{\mathbf{k}}$, the 4PF in the particular ordering channel can be written as a bilinear expression $\sum_{\mathbf{k},\mathbf{p}} W^\Lambda(\mathbf{k},\mathbf{p})O^\dagger_{\mathbf{k}}O_{\mathbf{p}}$, where W^Λ are the channel couplings. The 4PF, for instance, in the Cooper channel, is then decomposed into different eigenmode contributions,

$$W^{\Lambda,\mathrm{SC}}(\mathbf{k},\mathbf{p}) = \sum_i w_i^{\mathrm{SC}}(\Lambda) f_i^{\mathrm{SC}*}(\mathbf{k}) f_i^{\mathrm{SC}}(\mathbf{p}), \tag{2}$$

where i is a symmetry decomposition running index, and the leading instability of that channel corresponds to an

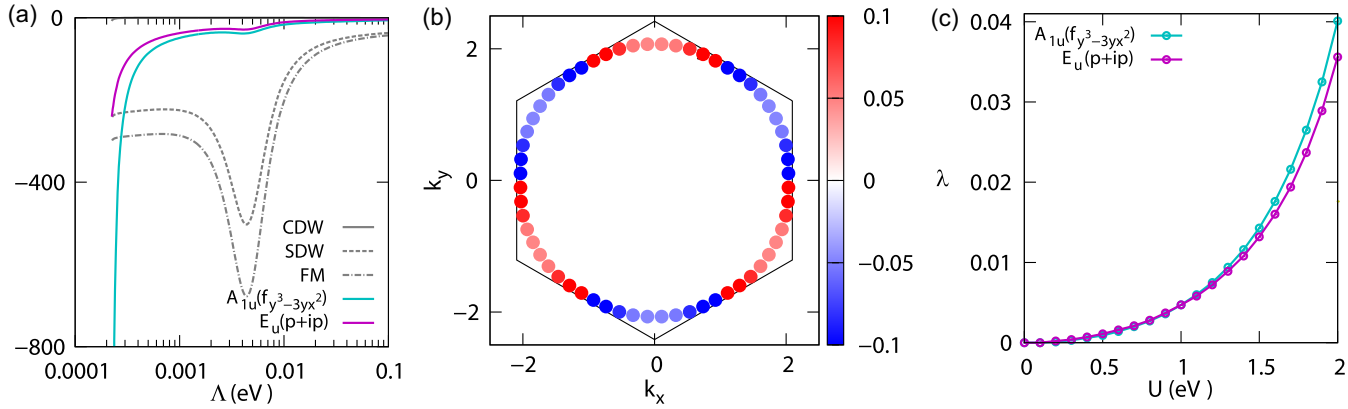

FIG. 4. Superconducting instability. (a) Typical fRG flow of the Fermi surface particle-particle and particle-hole instabilities when the chemical potential is set slightly below the vHs as a function of the infrared cutoff Λ ($\max|V_{\Lambda=W}(\mathbf{k}_1,\mathbf{k}_2,\mathbf{k}_3,\mathbf{k}_4)| = 2.0$ eV). The superconducting channels of the mean-field decomposition are labeled according to the irreducible representations of D_{3d} they transform to. The charge density wave (CDW) channel is orders of magnitude smaller than the other channels, and as such hardly visible. (b) Modulation of the superconducting gap of the leading f-wave instability along the Fermi surface (arb. units). (c) Typical RPA results at the vHs as a function of the intraorbital repulsion U at fixed $J/U = 0.2$ ratio. λ's are the eigenvalues of the RPA pairing vertex [23].

eigenvalue $w_1^{\mathrm{SC}}(\Lambda)$ first diverging under the flow of Λ. $f_i^{\mathrm{SC}}(\mathbf{k})$ is the superconducting form factor of pairing mode i which tells us about the superconducting pairing symmetry and hence the gap structure associated with it.

We use the same Hamiltonian within a multiband random phase approximation (RPA) fluctuation exchange approximation scheme [27] in order to provide an independent validation of our fRG results. Note that spin-orbit coupling (SOC) and the Rashba interaction have not been taken into account, which promotes a more efficient implementation. This assumption is justified for germanene: As a recent theoretical study demonstrates, in Ge/MoS_2 the layer/substrate interaction sensibly reduces the influence of SOC compared to the freestanding case [28]. Moreover, we focus on a correlation driven scenario, neglecting in the interaction Hamiltonian Eq. (1) any coupling with a deformable lattice.

Near the vHs, we find a prominent superconducting instability in the spin triplet sector, since the renormalized vertex V_Λ diverges in this channel as Λ approaches in the fRG flow the Fermi level [see Fig. 4(a)]. The leading pairing state transforms according to the A_{1u} irreducible representation of D_{3d}, i.e., the point group symmetry of the buckled geometry of germanene. Imposing a mean-field decoupling in the diverging vertex channel [29], we find that the gap function $\Delta_{\mathbf{k}}$ associated to the leading instability shows a $f_{y(y^2-3x^2)}$ profile, where the gap function changes sign every 60° rotation and has line nodes along the $k_y = 0$, $k_y = \pm\sqrt{3}k_x$ lines [see Fig. 4(b)]. The fRG results are validated by RPA fluctuation exchange calculations, the results of which we show in Fig. 4(c), where we also find the dominant pairing state to be located in the A_{1u} lattice group representation (see Ref. [23] for details).

As the Fermi pocket is rather circular and does not exhibit a particularly peaked momentum structure of the DOS at the Fermi level, the $\mathbf{q} = \mathbf{0}$ particle-hole fluctuation channel is dominant. This naturally promotes the tendency towards triplet pairing, where all subchannels satisfy the condition that the gap function connected by the nesting vector $\mathbf{q}$ [see Fig. 3(a)] must have the same sign. This is a recurrent motif from other theoretical proposals for f-wave superconductivity, such as employing the sublattice interference in a kagome metal [30], or the incommensurate spin fluctuations at moderate momenta in twisted bilayer graphene near the 1/4 filling [31]. Moreover, the nondiverging flow in the particle-hole channels also points to a smooth nondiverging behavior (as a function of doping) of the electronic screening function ε^{-1}. Since the latter determines the effective potential and forces acting on the ions, it is likely to expect that Ge/MoS_2 remains stable and nonmagnetic upon charge doping.

Within the triplet channel, microscopic details such as the hexagonal symmetry then yield a preference of the f-wave state over other candidates states such as the p-wave state, which is the subleading instability both at the fRG and RPA level. We also note that the competition between the f- and p-wave instability can to some extent be tuned by varying the J/U ratio in the interaction Hamiltonian. This is an interesting perspective if we assume that the Hund's coupling can be tailored by substrate engineering [32]. The agreement between fRG and RPA significantly supports the prediction of f-wave triplet superconductivity in Ge/MoS_2. This is because, within RPA, it might sometimes occur that the relevance of ferromagnetic fluctuations is overestimated. At the instance of LiFeAs, early RPA studies had predicted p-wave superconductivity [33], whereas fRG found a dominant extended s wave which agreed with the eventually converging picture from experimental evidence [34].

IV. CONCLUSIONS

Our combined *ab initio*, RPA, and fRG analysis finds that the recently synthesized 2D-Xene Ge/MoS_2 is a promising platform for studying unconventional Fermi surface instabilities, in light of triplet superconductivity. In order to reach the scenario outlined here, further steps of experimental refinement suggest themselves to be followed up on. First, there appears to be an electronic level mismatch between the

current Ge/MoS_2 in experiment and the *ab initio* simulations, possibly due to nonsaturated defects [20]. Second, to avoid detrimental disorder effects from chemical doping, one might want to pursue electrostatic doping from gating methods. Recent experiments have achieved a doping in MoS_2 of $\sim 1.2 \times 10^{14}$ cm^{-2} carrier density [35], which, if transferred to germanene, would correspond to ~ 0.08 electrons. At this doping level, our calculations already suggest a propensity towards a $f_{x(x^2-3y^2)}$-wave instability, even though higher doping would still be desirable. From a broader perspective, this is only the beginning to employ *substrate engineering* towards accomplishing exotic Fermi surface instabilities. As significant progress has already been made at the frontier of substrate-assisted topological insulators [14], we hope that our work will stimulate similar efforts for unconventional superconductivity in layer/substrate heterostructures.

ACKNOWLEDGMENTS

This work was supported by the DFG through SFB1170 "ToCoTronics" (Project B04) and the Würzburg-Dresden Cluster of Excellence ct.qmat on Complexity and Topology in Quantum Matter. We gratefully acknowledge the Gauss Centre for Supercomputing e.V. (www.gauss-centre.eu) for funding this project by providing computing time on the GCS Supercomputer SuperMUC at Leibniz Supercomputing Centre (www.lrz.de).

[1] A. H. Castro Neto, F. Guinea, N. M. R. Peres, K. S. Novoselov, and A. K. Geim, Rev. Mod. Phys. **81**, 109 (2009).
[2] A. K. Geim and K. S. Novoselov, Nat. Mater. **6**, 183 (2007).
[3] C. L. Kane and E. J. Mele, Phys. Rev. Lett. **95**, 226801 (2005).
[4] F. D. M. Haldane, Phys. Rev. Lett. **61**, 2015 (1988).
[5] Y. Cao, V. Fatemi, S. Fang, K. Watanabe, T. Taniguchi, E. Kaxiras, and P. Jarillo-Herrero, Nature (London) **556**, 43 (2018).
[6] D. M. Kennes, J. Lischner, and C. Karrasch, Phys. Rev. B **98**, 241407(R) (2018).
[7] I. E. Dzyaloshinskii, Sov. Phys. JETP **66**, 848 (1987).
[8] R. Nandkishore, L. S. Levitov, and A. V. Chubukov, Nat. Phys. **8**, 158 (2012).
[9] M. L. Kiesel, C. Platt, W. Hanke, D. A. Abanin, and R. Thomale, Phys. Rev. B **86**, 020507(R) (2012).
[10] W.-S. Wang, Y.-Y. Xiang, Q.-H. Wang, F. Wang, F. Yang, and D.-H. Lee, Phys. Rev. B **85**, 035414 (2012).
[11] J. L. McChesney, A. Bostwick, T. Ohta, T. Seyller, K. Horn, J. González, and E. Rotenberg, Phys. Rev. Lett. **104**, 136803 (2010).
[12] C.-C. Liu, W. Feng, and Y. Yao, Phys. Rev. Lett. **107**, 076802 (2011).
[13] Y. Xu, B. Yan, H.-J. Zhang, J. Wang, G. Xu, P. Tang, W. Duan, and S.-C. Zhang, Phys. Rev. Lett. **111**, 136804 (2013).
[14] F. Reis, G. Li, L. Dudy, M. Bauernfeind, S. Glass, W. Hanke, R. Thomale, J. Schäfer, and R. Claessen, Science **357**, 287 (2017).
[15] A. Molle, J. Goldberger, M. Houssa, Y. Xu, S.-C. Zhang, and D. Akinwande, Nat. Mater. **16**, 163 (2017).
[16] P. Vogt, P. De Padova, C. Quaresima, J. Avila, E. Frantzeskakis, M. C. Asensio, A. Resta, B. Ealet, and G. Le Lay, Phys. Rev. Lett. **108**, 155501 (2012).
[17] A. Fleurence, R. Friedlein, T. Ozaki, H. Kawai, Y. Wang, and Y. Yamada-Takamura, Phys. Rev. Lett. **108**, 245501 (2012).
[18] M. E. Dávila, L. Xian, S. Cahangirov, A. Rubio, and G. Le Lay, New J. Phys. **16**, 095002 (2014).
[19] F. d'Acapito, S. Torrengo, E. Xenogiannopoulou, P. Tsipas, J. Marquez Velasco, D. Tsoutsou, and A. Dimoulas, J. Phys.: Condens. Matter **28**, 045002 (2016).
[20] L. Zhang, P. Bampoulis, A. N. Rudenko, Q. Yao, A. van Houselt, B. Poelsema, M. I. Katsnelson, and H. J. W. Zandvliet, Phys. Rev. Lett. **116**, 256804 (2016).
[21] D. Di Sante, P. Eck, M. Bauernfeind, M. Will, R. Thomale, J. Schäfer, R. Claessen, and G. Sangiovanni, Phys. Rev. B **99**, 035145 (2019).
[22] F.-F. Zhu, W.-J. Chen, Y. Xu, C.-L. Gao, D.-D. Guan, C.-H. Liu, D. Qian, S.-C. Zhang, and J.-F. Jia, Nat. Mater. **14**, 1020 (2015).
[23] See Supplemental Material at http://link.aps.org/supplemental/10.1103/PhysRevB.99.201106 for details on the tight-binding models, as well as DFT, RPA, and fRG calculations, which includes Refs. [25–27,36–46].
[24] C.-C. Liu, H. Jiang, and Y. Yao, Phys. Rev. B **84**, 195430 (2011).
[25] W. Metzner, M. Salmhofer, C. Honerkamp, V. Meden, and K. Schönhammer, Rev. Mod. Phys. **84**, 299 (2012).
[26] C. Platt, W. Hanke, and R. Thomale, Adv. Phys. **62**, 453 (2013).
[27] N. E. Bickers, D. J. Scalapino, and S. R. White, Phys. Rev. Lett. **62**, 961 (1989).
[28] T. Amlaki, M. Bokdam, and P. J. Kelly, Phys. Rev. Lett. **116**, 256805 (2016).
[29] J. Reiss, D. Rohe, and W. Metzner, Phys. Rev. B **75**, 075110 (2007).
[30] M. L. Kiesel, C. Platt, and R. Thomale, Phys. Rev. Lett. **110**, 126405 (2013).
[31] Q.-K. Tang, L. Yang, D. Wang, F.-C. Zhang, and Q.-H. Wang, Phys. Rev. B **99**, 094521 (2019).
[32] A. A. Khajetoorians, M. Valentyuk, M. Steinbrecher, T. Schlenk, A. Shick, J. Kolorenc, A. I. Lichtenstein, T. O. Wehling, R. Wiesendanger, and J. Wiebe, Nat. Nanotechnol. **10**, 958 (2015).
[33] P. M. R. Brydon, M. Daghofer, C. Timm, and J. van den Brink, Phys. Rev. B **83**, 060501(R) (2011).
[34] C. Platt, R. Thomale, and W. Hanke, Phys. Rev. B **84**, 235121 (2011).
[35] J. T. Ye, Y. J. Zhang, R. Akashi, M. S. Bahramy, R. Arita, and Y. Iwasa, Science **338**, 1193 (2012).
[36] G. Kresse and J. Furthmüller, Phys. Rev. B **54**, 11169 (1996).
[37] G. Kresse and D. Joubert, Phys. Rev. B **59**, 1758 (1999).
[38] P. E. Blöchl, Phys. Rev. B **50**, 17953 (1994).
[39] J. P. Perdew, K. Burke, and M. Ernzerhof, Phys. Rev. Lett. **77**, 3865 (1996).
[40] W. Ku, T. Berlijn, and C.-C. Lee, Phys. Rev. Lett. **104**, 216401 (2010).

[41] M. Tomić, H. O. Jeschke, and R. Valentí, Phys. Rev. B **90**, 195121 (2014).

[42] C. Platt, R. Thomale, C. Honerkamp, S.-C. Zhang, and W. Hanke, Phys. Rev. B **85**, 180502(R) (2012).

[43] A. F. Kemper, T. A. Maier, S. Graser, H.-P. Cheng, P. J. Hirschfeld, and D. J. Scalapino, New J. Phys. **12**, 073030 (2010).

[44] X. Wu, J. Yuan, Y. Liang, H. Fan, and J. Hu, Europhys. Lett. **108**, 27006 (2014).

[45] X. Wu, F. Yang, C. Le, H. Fan, and J. Hu, Phys. Rev. B **92**, 104511 (2015).

[46] C. Lu, L.-D. Zhang, X. Wu, F. Yang, and J. Hu, Phys. Rev. B **97**, 165110 (2018).